Frontiers of Information Technology & Electronic Engineering
www.jzus.zju.edu.cn; engineering.cae.cn; www.springerlink.com
ISSN 2095-9184 (print); ISSN 2095-9230 (online)
E-mail: jzus@zju.edu.cn

Correspondence:

A high-isolation coupled-fed building block for metal-rimmed 5G smartphones*

Aidi REN[†‡1], Chengwei YU[1], Lixia YANG[1], Wei CUI[2], Zhixiang HUANG[1], Ying LIU[3]

[1]*Information Materials and Intelligent Sensing Laboratory of Anhui Province, Anhui University, Hefei 230601, China*

[2]*Aviation Key Laboratory of Science and Technology on Electromagnetic Environmental Effects, Shenyang 110000, China*

[3]*Science and Technology on Antenna and Microwave Laboratory, Xidian University, Xi'an 710071, China*

[†]E-mail: renaidi@ahu.edu.cn

Received Mar. 23, 2023; Revision accepted Aug. 22, 2023; Crosschecked Oct. 26, 2023

https://doi.org/10.1631/FITEE.2300203

A dual-antenna building block with high isolation is presented for metal-rimmed fifth-generation (5G) smartphones. A coupled-fed loop antenna and a coupled-fed slot antenna based on a simple T-slot etched on the ground plane are meticulously designed to form a compact building block. Notably, although the coupled-fed loop antenna and the coupled-fed slot antenna share the same aperture, a desirable isolation of >30 dB is exhibited. Afterward, an 8×8 multiple-input multiple-output (MIMO) system is achieved by integrating four such dual-antenna building blocks. The measured mutual coupling and envelope correlation coefficients (ECCs) of the presented 8×8 MIMO system are <−18.5 dB and <0.02, respectively.

1 Introduction

Recently, MIMO technology has been extensively exploited in 5G terminals, as the channel capacity is proportional to the number of antennas (Hong, 2017). Nevertheless, due to the arrangement of many MIMO antennas operating in the same bands within a space-limited smartphone, the interference between antennas is a fierce issue that suppresses the data rate. Furthermore, the more the elements placed, the more critical the interference. In consequence, alleviating mutual coupling and reducing the element size are crucial for a 5G MIMO system.

Various methods have been introduced to mitigate interference (Zhang XX et al., 2020). Amid these decoupling techniques, modifying ground planes, such as defected ground structure (DGS) (Hei et al., 2021) and etched slots (Jiang et al., 2019), have been used to mitigate mutual coupling. Besides, integrating additional structures, including a neutralization line (Guo et al., 2018), decoupling branches (Luo et al., 2022), and so on, can suppress interference effectively. Metamaterials are also used to enhance isolation by reducing the coupling current (Sultan et al., 2020). To reduce the size of the decoupling structure, decoupling based on lumped elements has been investigated (Ye et al., 2022). The methods mentioned above need to introduce external structures to enhance isolation, which takes up extra space. To simplify MIMO systems, antennas with self-isolated characteristics have been studied (Ren ZY et al., 2019). Besides, polarization diversity techniques (Li MY et al., 2016), characteristic mode theory (CMT) (Liu et al., 2019; Hu et al., 2022),

‡ Corresponding author

* Project supported by the National Natural Science Foundation of China (No. 62201006) and the China Postdoctoral Science Foundation (No. 2022M722961)

ORCID: Aidi REN, https://orcid.org/0000-0002-0600-4550; Lixia YANG, https://orcid.org/0000-0002-7943-9846

stable null points (Zhao et al., 2018; Ren AD et al., 2019b), and elements with reduced grounding effect (Li YX et al., 2019) have been investigated. Furthermore, the requirement of further miniaturization has accelerated the investigation of multi-antenna pairs (Wong et al., 2017; Ren AD et al., 2019a; Sun et al., 2020; Chang et al., 2022; Hu et al., 2023).

The increased strength, durability, metallic luster, and stylish exterior have made the metal bezel attractive to customers. However, the existence of the metal bezel blocks the radiation of electromagnetic fields. Therefore, many researchers have been committed to the coexistence of MIMO systems with the metal bezel. Isolation of >13 dB is achieved by properly selecting the slot positions (Chen et al., 2019). An antenna pair composed of two tightly arranged open-slot antennas has been presented, offering only an isolation of >10 dB by using a connecting line (Sun et al., 2021). The CMT has been used to find the desired modes and optimal feeding positions (Luomaniemi et al., 2021). As a result, a four-element MIMO system for 5G communication with isolation >10 dB is obtained. The CMT is used to implement a MIMO system with a low specific absorption rate (SAR) and high isolation (>15.4 dB) for metal-rimmed smartphones (Zhang HH et al., 2022). However, only four elements are integrated into a smartphone, which limits the improvement of channel capacity. A dual-antenna building block based on a suspended metal strip is realized by selectively exciting the half-wavelength and wavelength dipole-type mode, integrating only four elements (Qu and Piao, 2022). An eight-unit MIMO system was proposed for a full metal-framed tablet device. To mitigate mutual coupling, solution capacitance was used to suppress the traveling wave (12.94 dB) (Fang et al., 2022).

In this paper, a dual-antenna building block is designed, in which a coupled-fed loop antenna and a coupled-fed slot antenna occupy the same T-shaped slot. Note that the building block without integration of any external decoupling structure not only has a small size but also yields up to 30 dB of isolation. Then, a compact 8×8 MIMO system constructed by four dual-antenna building blocks for 5G metal bezel smartphone applications is designed and fabricated. Ultimately, measurement is conducted and the measurement results are presented and discussed.

2 Compact MIMO array design

2.1 Coupled-fed dual-antenna module

2.1.1 Structure and performances of the proposed dual-antenna building block

Fig. 1 is the structural diagram of the dual-antenna building block. As shown in Fig. 1, the FR4 substrate with a relative dielectric constant of 4.4 is adopted as the system main board, and the specific size is 145 mm× 75 mm×0.8 mm. The detailed structure of the dual-antenna module is given in the dashed boxes in the figure. It can be observed that the structure is very simple, consisting of a T-shaped open slot engraved on the ground plane, a chip inductor (6.2 nH), and two L-shaped feed branches printed on the top surface of the system board. The inductor is placed at the opening gap of the slot, and the thickness and height of the metal frame are 0.6 mm and 6.0 mm, respectively, with a 1-mm break at the opening gap. Clearances of 5 mm are retained on both sides of the system main board for placing components such as 2G, 3G, and 4G antennas.

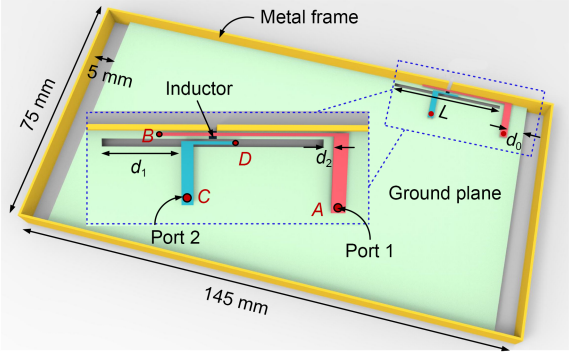

Fig. 1 Structure of the compact building block (L=28.1 mm, d_0=2.50 mm, d_1=10.15 mm, d_2=2.05 mm)

When the feed port of the coupled-fed loop antenna (port 1) is fed, the surface current around the open slot is loop shaped, and the coupled-fed loop antenna (antenna 1) works at this time. The break on the metal frame can effectively improve the matching level of the coupled-fed loop antenna. The chip inductor is also used to improve the impedance matching of the coupled-fed loop antenna. When the feed port of the coupled-fed slot antenna (port 2) is fed, the coupled-fed slot antenna (antenna 2) works. The L-shaped

coupled-fed branch *AB* is composed of vertical and horizontal components; the size of the vertical part is 9.6 mm×1.8 mm, and the size of the horizontal part is 21.9 mm×0.4 mm. The L-shaped coupled-fed branch *CD* is composed of vertical and horizontal components; the size of the vertical part is 7.6 mm×1.5 mm, and the size of the horizontal part is 5.25 mm×0.4 mm. The width of the designed compact building block is only 1 mm (0.012λ at 3.50 GHz, with λ being wavelength), and the feeding structure is also very simple, which makes it easy to implement in engineering.

Fig. 2 gives the simulated *S*-parameter curves of the dual-antenna module. It can be seen from Fig. 2 that the reflection coefficients of the two antennas in the 3.40–3.60 GHz frequency band are <−6 dB. It is noteworthy that the isolation between the two antennas is >30 dB. Fig. 3 gives the simulated ECC curve of the building block. It can be seen that the ECC of the two antennas is <0.02 in the entire working frequency band.

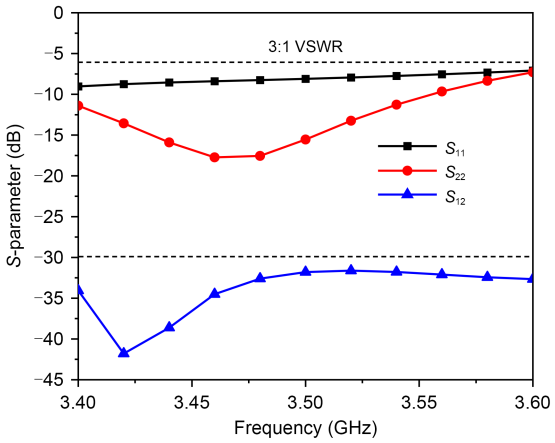

Fig. 2 Simulated *S*-parameters for the dual-antenna module (VSWR: voltage standing wave ratio)

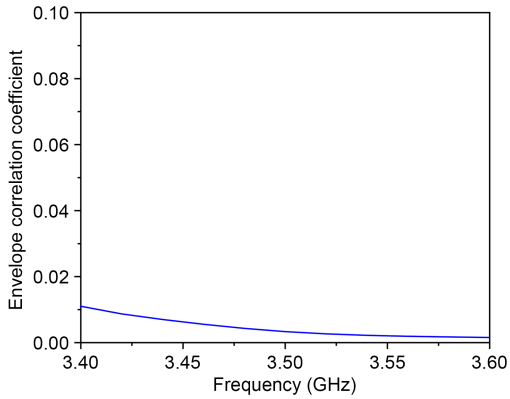

Fig. 3 Simulated envelope correlation coefficient for the dual-antenna building block

2.1.2 Decoupling analysis

The decoupling mechanism of the proposed building block is investigated in Figs. 4 and 5. The vector current distributions when the two antennas work separately in the building block are shown in Fig. 4. According to Fig. 4a, when antenna 1 is working, the current on the ground plane flows mainly along the longer side of the ground, and the current distribution around the rectangular slot on the ground plane is a loop. According to Fig. 4b, it can be seen that the current on the ground is mainly vertical to the longer side of the ground plane when antenna 2 is working. It can be concluded from Fig. 4 that the ground currents induced by antennas 1 and 2 are almost orthogonal, reducing the coupling from the ground plane effectively. The current distribution around the building block induced by the loop antenna and slot antenna is also orthogonal.

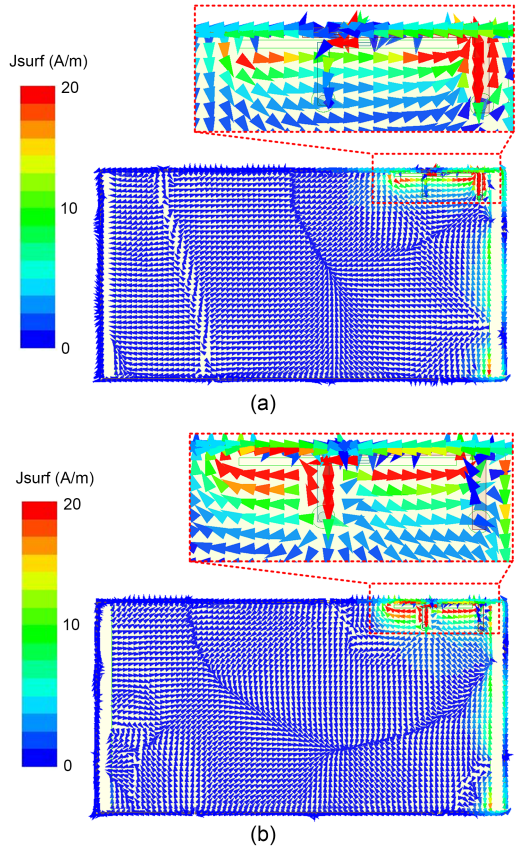

Fig. 4 Simulated vector current distributions at 3.50 GHz when antenna 1 (a) or antenna 2 (b) is fed

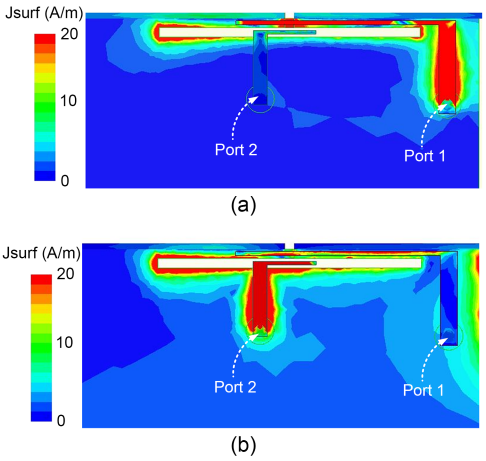

Fig. 5 Simulated current amplitude distributions at 3.50 GHz when antenna 1 (a) or antenna 2 (b) is fed

Fig. 5 gives the current amplitude distributions when antennas 1 and 2 work separately. As Fig. 5a depicts, when antenna 1 works, port 1 is fed, and the current distribution around port 2 is very weak. From Fig. 5b, it can be observed that during the operation of antenna 2, port 2 is excited, and the current distribution at port 1 is very weak. Consequently, there are three reasons to explain the high isolation level for the proposed dual-antenna module:

1. Because ground currents induced by antennas 1 and 2 are orthogonal, the coupling from the ground plane is effectively mitigated.

2. The current distributions around the dual-antenna module caused by antennas 1 and 2 are also orthogonal.

3. When the two antennas work separately, the current flowing into the other antenna feed port is very weak.

2.1.3 Parametric study

Since the two antennas in the designed dual-antenna module occupy the same T-shaped open slot, the length L of the slot is a very important parameter, affecting the resonance frequencies of antennas 1 and 2 at the same time.

Fig. 6 shows the simulated S-parameter curves of the dual-antenna module when L increases from 27.9 to 28.3 mm with an interval of 0.2 mm. As shown in Fig. 6a, as L increases, the resonance frequency of antenna 1 shifts to a lower frequency. As observed from Fig. 6b, when L increases from 27.9 to 28.3 mm,

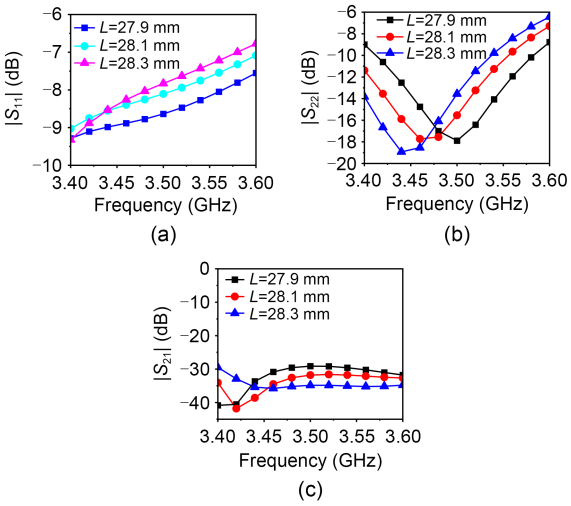

Fig. 6 *S*-parameters of the building block with different lengths: (a) reflection coefficient of antenna 1; (b) reflection coefficient of antenna 2; (c) transmission coefficient (*L*: length of the slot)

the resonance frequency of antenna 2 shifts to a lower frequency, from 3.50 to 3.45 GHz. Further observing Fig. 6c, the isolation between the two units is the best when L is 28.1 mm. Therefore, the final length L is selected to be 28.1 mm.

Fig. 7 depicts the influence of inductance on the performance of the building block. Fig. 7 shows that the S-parameter curves of the building block change when the inductance values are changed. As shown in Fig. 7a, when the inductance value is increased from

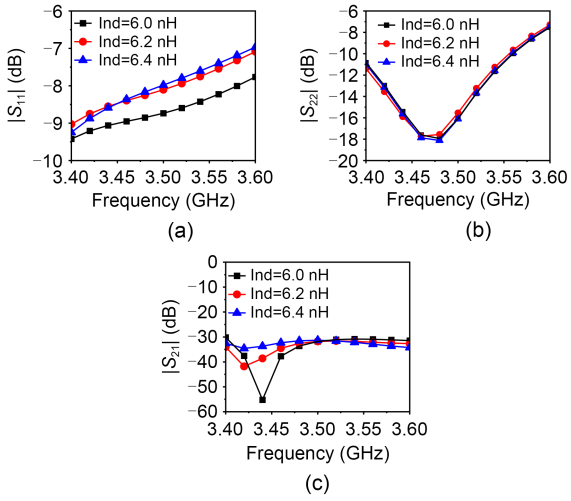

Fig. 7 *S*-parameters of the building block with different inductance values: (a) reflection coefficient of antenna 1; (b) reflection coefficient of antenna 2; (c) transmission coefficient (Ind: inductance)

6.0 to 6.4 nH, the resonance frequency of antenna 1 shifts toward a lower frequency. Observing Fig. 7b, when the inductance value increases, the resonance frequency of antenna 2 almost remains unchanged. When the inductance value is 6.2 nH, the isolation between the two antennas is optimal, and the isolation level is >30 dB. Therefore, the inductance value is finally selected as 6.2 nH.

2.2 Eight-element MIMO array antenna

2.2.1 Eight-element MIMO array structure and performances

An eight-element MIMO is implemented based on the coupled-fed dual-antenna building block. Fig. 8 shows the detailed structure of the MIMO system. The 8×8 MIMO system has a symmetrical structure that is composed of four completely identical dual-antenna modules. To improve the performance of the 8×8 MIMO array, the sizes of the two blocks are changed to some extent.

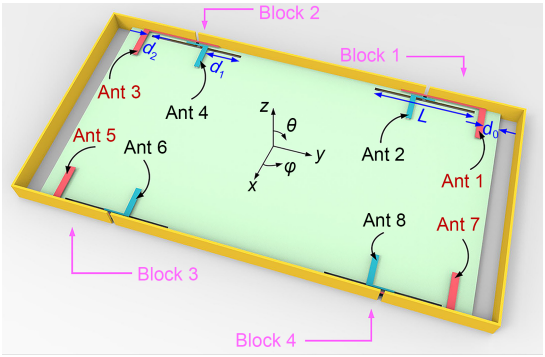

Fig. 8 Configuration of the proposed eight-element MIMO system (L=28.1 mm, d_0=5.10 mm, d_1=9.55 mm, d_2=1.65 mm)

The simulated S-parameters of the proposed eight-element MIMO array are depicted in Fig. 9. Due to the symmetry of the MIMO system, only part of the antenna performance is shown. According to Fig. 9, the reflection coefficients of all elements are <−6 dB in the frequency band 3.40–3.60 GHz. Further observing Fig. 9, due to the coupling between different modules and the changes in some parameters, the isolation of two antennas in the same building block is >29 dB, and the isolation of two elements between different modules (such as between antennas 1 and 7, between antennas 1 and 3, and so on) is >18.5 dB. The isolations between antennas 1 and 7, and between antennas 1

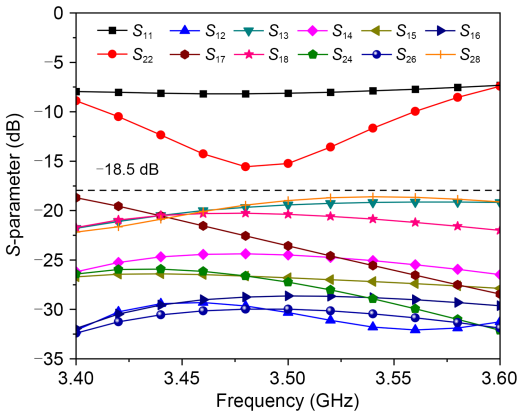

Fig. 9 Simulated S-parameters of the eight-element MIMO system

and 3 in different modules are lower than the isolation in the same module. This phenomenon is reasonable because the polarizations of antennas 1 and 7 (antennas 1 and 3, and so on) in different modules are the same.

2.2.2 Experimental results and discussion

To evaluate the performance of the designed eight-element MIMO system, we process and measure the MIMO array, and the physical diagram of the eight-element MIMO system is depicted in Fig. 10. The top and bottom views of the physical eight-element MIMO array are presented in Figs. 10a and 10b, respectively.

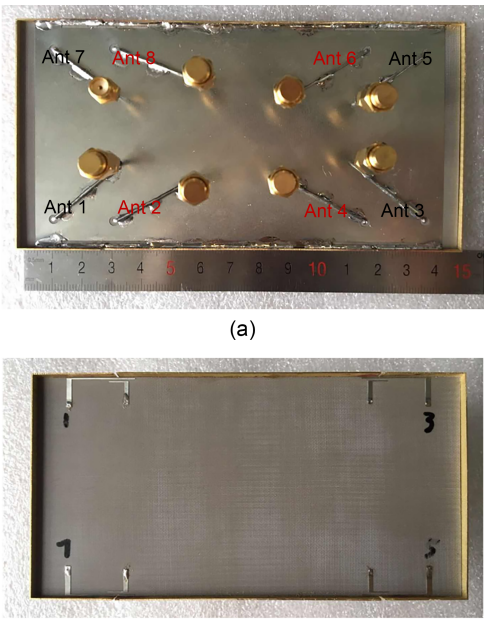

Fig. 10 Fabricated eight-element MIMO array: (a) top view; (b) bottom view

The measured *S*-parameters of the eight-element MIMO array are presented in Fig. 11. The reflection coefficients for both antennas 1 and 2 are <−6 dB in the frequency band of 3.40–3.60 GHz, and the measured isolation of the whole MIMO system is >18.5 dB. Observing Figs. 9 and 11, the simulated *S*-parameters of the eight-element MIMO array agree very well with the measurement results.

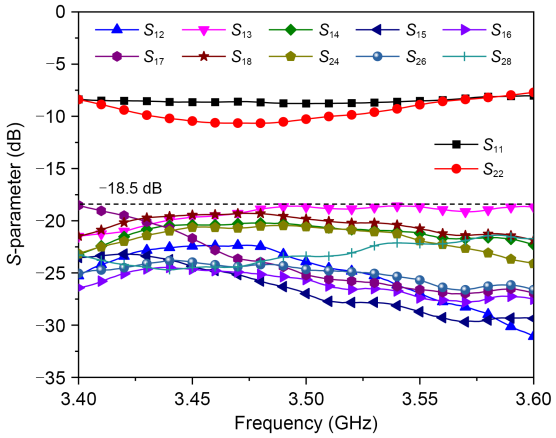

Fig. 11 Measured *S*-parameters of the eight-element MIMO system

Fig. 12 shows the measured efficiency of the MIMO system; the efficiency of the antenna varies from 43% to 54% over the entire frequency band, which fully meets the actual application requirements.

Fig. 13 gives both the measured and simulated normalized radiation patterns for antennas 1 and 2 at 3.50 GHz. When one antenna is measured, the other ports match well to a 50-Ω matched load. It can be seen from Fig. 13 that the measured patterns of the

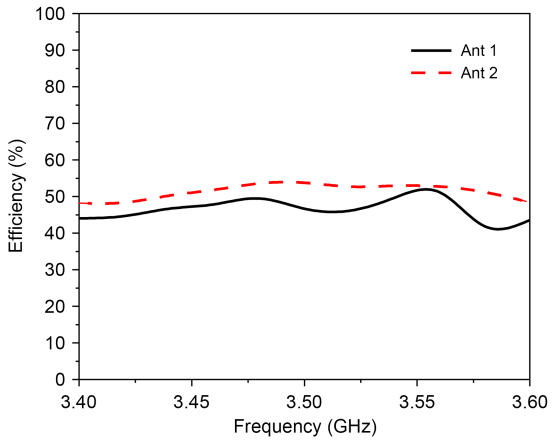

Fig. 12 Measured radiation efficiencies

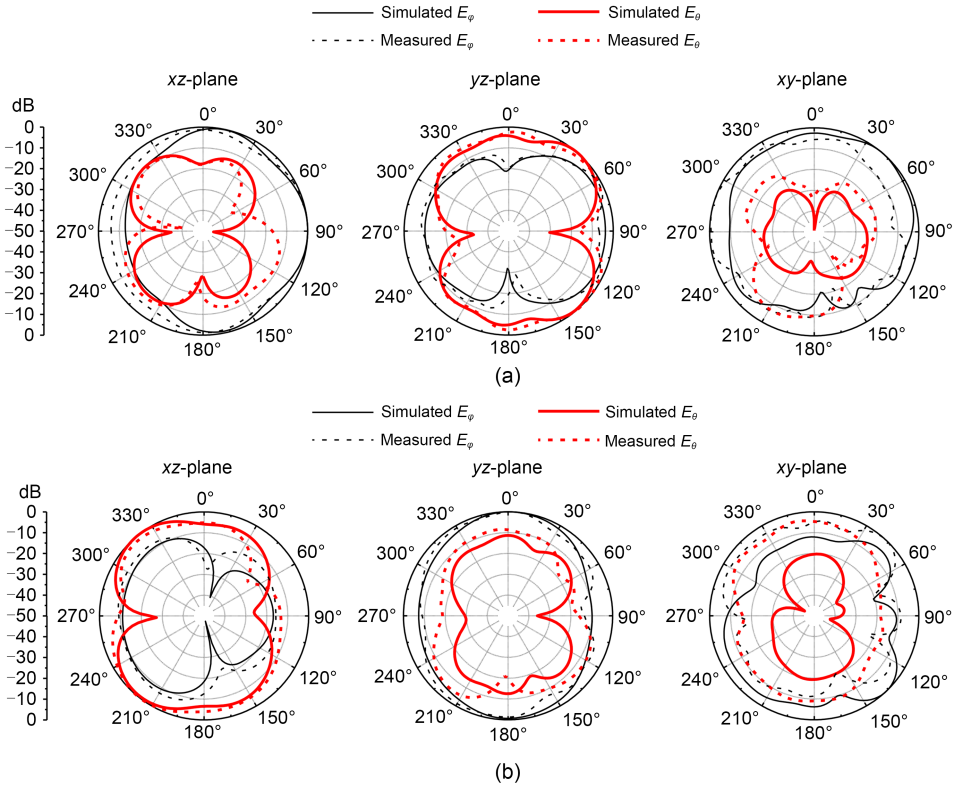

Fig. 13 Normalized radiation patterns: (a) antenna 1 at 3.50 GHz; (b) antenna 2 at 3.50 GHz

eight-element MIMO array are in good agreement with the simulated patterns.

According to the measured three-dimensional (3D) radiation patterns, the ECCs are calculated and given in Fig. 14. From Fig. 14, the ECCs of the eight-element MIMO system are <0.02 in the entire working frequency band, which indicates that the designed eight-element MIMO array antenna has good MIMO performance.

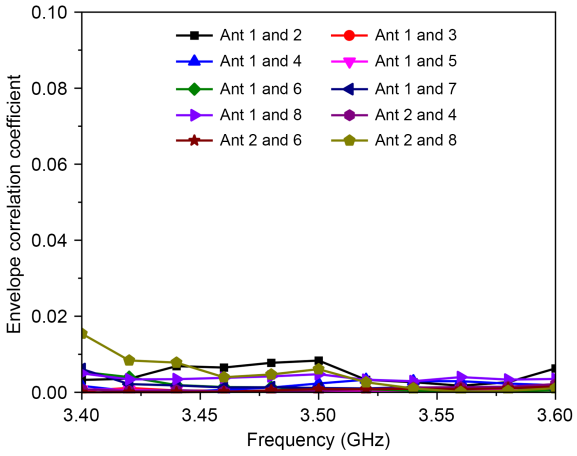

Fig. 14 Measured envelope correlation coefficients for the eight-element MIMO system

The comparison between the referential designs and our study is presented in Table 1 to reveal the merits of our design. The size of the antenna pair provided by Hei et al. (2021) is far larger than that in this study. Moreover, these designs cannot be applied in smartphones with a metal frame (Hei et al., 2021; Ye et al., 2022). Ren AD et al. (2019a) proposed a MIMO system with a metal frame. However, the isolation, ECC, and size of this study are better than those in the design presented by Ren AD et al. (2019a). Sun et al. (2021) provided a MIMO system with a wider band of 3.3–5.0 GHz. However, the isolation is only >10 dB, which is much lower than that (>18.5 dB) in this study. The elements in the MIMO systems proposed by Fang et al. (2022) and Zhang HH et al. (2022) are arranged separately, which leads to a large size. Ultimately, the present study provides good isolation, better ECC, and small size, simultaneously.

3 Conclusions

A compact coupled-fed dual-antenna building block has been constructed in this study. The building block is simple in structure and easy to process, and has a high degree of isolation. The dual-antenna building block is composed of a coupled-fed loop antenna and a coupled-fed slot antenna that completely overlap. Based on this dual-antenna module, an eight-element MIMO system is designed, and the fabricated eight-element MIMO array is measured. The measured isolation of the designed eight-element MIMO system is >18.5 dB without any decoupling element. In addition, the MIMO array has good measured efficiencies, with a measured efficiency variation range of 43%–54% in the entire working frequency band. The measured ECC of the MIMO system is <0.02. Therefore, the designed MIMO array has great potential in 5G metal-rimmed mobile phone applications.

Contributors

Aidi REN designed the research. Aidi REN and Chengwei YU processed the data. Chengwei YU drafted the paper. Lixia YANG, Wei CUI, and Zhixiang HUANG helped organize the paper. Aidi REN and Ying LIU revised and finalized the paper.

Compliance with ethics guidelines

Aidi REN, Chengwei YU, Lixia YANG, Wei CUI, Zhixiang HUANG, and Ying LIU declare that they have no conflict of interest.

Table 1 Comparison of the presented and referential antennas

Reference	Bandwidth (GHz)	Isolation (dB)	ECC	Dimension of a pair (mm×mm×mm)	Metal frame
Hei et al., 2021	3.30–5.95	>15	<0.11	34.6×6×0.8	Without
Ye et al., 2022	3.42–3.69	>24	<0.01	16×6×0.8	Without
Ren AD et al., 2019a	3.4–3.6	>16	<0.05	28.4×1×0.8	With
Sun et al., 2021	3.3–5.0	>10	<0.30	24×2×5	With
Zhang HH et al., 2022	3.4–3.6	>15.4	<0.07	N/A	With
Fang et al., 2022	3.4–3.6	>20.1	<0.17	N/A	With
This study	3.4–3.6	>18.5	<0.02	28.1×1×0.8	With

ECC: envelope correlation coefficient; N/A: not available

Data availability

The data that support the findings of this study are available from the corresponding author upon reasonable request.

References

Chang L, He WB, Chen XM, et al., 2022. Zero ground clearance dual antenna pair for metal-cased fifth-generation multiple input multiple output smartphone. *Front Inform Technol Electron Eng*, 23(10):1562-1567. https://doi.org/10.1631/FITEE.2200119

Chen QG, Lin HW, Wang JP, et al., 2019. Single ring slot-based antennas for metal-rimmed 4G/5G smartphones. *IEEE Trans Antenn Propag*, 67(3):1476-1487. https://doi.org/10.1109/tap.2018.2883686

Fang YX, Liu Y, Jia YT, et al., 2022. 5G SAR-reduction MIMO antenna with high isolation for full metal-rimmed tablet device. *IEEE Trans Antenn Propag*, 70(5):3846-3851. https://doi.org/10.1109/tap.2021.3137295

Guo JL, Cui L, Li C, et al., 2018. Side-edge frame printed eight-port dual-band antenna array for 5G smartphone applications. *IEEE Trans Antenn Propag*, 66(12):7412-7417. https://doi.org/10.1109/tap.2018.2872130

Hei YQ, He JG, Li WT, 2021. Wideband decoupled 8-element MIMO antenna for 5G mobile terminal applications. *IEEE Antenn Wirel Propag Lett*, 20(8):1448-1452. https://doi.org/10.1109/lawp.2021.3086261

Hong W, 2017. Solving the 5G mobile antenna puzzle: assessing future directions for the 5G mobile antenna paradigm shift. *IEEE Microw Mag*, 18(7):86-102. https://doi.org/10.1109/mmm.2017.2740538

Hu W, Chen Z, Qian L, et al., 2022. Wideband back-cover antenna design using dual characteristic modes with high isolation for 5G MIMO smartphone. *IEEE Trans Antenn Propag*, 70(7):5254-5265. https://doi.org/10.1109/tap.2022.3145456

Hu W, Li QS, Wu H, et al., 2023. Dual-band antenna pair with high isolation using multiple orthogonal modes for 5G smartphones. *IEEE Trans Antenn Propag*, 71(2):1949-1954. https://doi.org/10.1109/tap.2022.3233458

Jiang W, Liu B, Cui YQ, et al., 2019. High-isolation eight-element MIMO array for 5G smartphone applications. *IEEE Access*, 7:34104-34112. https://doi.org/10.1109/access.2019.2904647

Li MY, Ban YL, Xu ZQ, et al., 2016. Eight-port orthogonally dual-polarized antenna array for 5G smartphone applications. *IEEE Trans Antenn Propag*, 64(9):3820-3830. https://doi.org/10.1109/tap.2016.2583501

Li YX, Sim CYD, Luo Y, et al., 2019. High-isolation 3.5 GHz eight-antenna MIMO array using balanced open-slot antenna element for 5G smartphones. *IEEE Trans Antenn Propag*, 67(6):3820-3830. https://doi.org/10.1109/tap.2019.2902751

Liu Y, Ren AD, Liu H, et al., 2019. Eight-port MIMO array using characteristic mode theory for 5G smartphone applications. *IEEE Access*, 7:45679-45692. https://doi.org/10.1109/access.2019.2909070

Luo Y, Zhu L, Liu Y, et al., 2022. A decoupling structure without sacrificing antenna-element performance for 5G smartphone designs. *Int J RF Microw Comput-Aided Eng*, 32(9):e23258. https://doi.org/10.1002/mmce.23258

Luomaniemi R, Ylä-Oijala P, Lehtovuori A, et al., 2021. Designing hand-immune handset antennas with adaptive excitation and characteristic modes. *IEEE Trans Antenn Propag*, 69(7):3829-3839. https://doi.org/10.1109/tap.2020.3044640

Qu LY, Piao HY, 2022. A dual-port single-dipole MIMO antenna pair based on selective modal excitation for 5G metal-rimmed terminals. *IEEE Access*, 10:100208-100214. https://doi.org/10.1109/access.2022.3188017

Ren AD, Liu Y, Sim CYD, 2019a. A compact building block with two shared-aperture antennas for eight-antenna MIMO array in metal-rimmed smartphone. *IEEE Trans Antenn Propag*, 67(10):6430-6438. https://doi.org/10.1109/tap.2019.2920306

Ren AD, Liu Y, Yu HW, et al., 2019b. A high-isolation building block using stable current nulls for 5G smartphone applications. *IEEE Access*, 7:170419-170429. https://doi.org/10.1109/access.2019.2955495

Ren ZY, Zhao AP, Wu SJ, 2019. MIMO antenna with compact decoupled antenna pairs for 5G mobile terminals. *IEEE Antenn Wirel Propag Lett*, 18(7):1367-1371. https://doi.org/10.1109/lawp.2019.2916738

Sultan KS, Abdullah HH, Abdallah EA, et al., 2020. Metasurface-based dual polarized MIMO antenna for 5G smartphones using CMA. *IEEE Access*, 8:37250-37264. https://doi.org/10.1109/access.2020.2975271

Sun LB, Li Y, Zhang ZJ, et al., 2020. Self-decoupled MIMO antenna pair with shared radiator for 5G smartphones. *IEEE Trans Antenn Propag*, 68(5):3423-3432. https://doi.org/10.1109/tap.2019.2963664

Sun LB, Li Y, Zhang ZJ, 2021. Wideband integrated quad-element MIMO antennas based on complementary antenna pairs for 5G smartphones. *IEEE Trans Antenn Propag*, 69(8):4466-4474. https://doi.org/10.1109/tap.2021.3060020

Wong KL, Tsai CY, Lu JY, 2017. Two asymmetrically mirrored gap-coupled loop antennas as a compact building block for eight-antenna MIMO array in the future smartphone. *IEEE Trans Antenn Propag*, 65(4):1765-1778. https://doi.org/10.1109/tap.2017.2670534

Ye Y, Zhao X, Wang JY, 2022. Compact high-isolated MIMO antenna module with chip capacitive decoupler for 5G mobile terminals. *IEEE Antenn Wirel Propag Lett*, 21(5):928-932. https://doi.org/10.1109/lawp.2022.3152236

Zhang HH, Liu XZ, Cheng GS, et al., 2022. Low-SAR four-antenna MIMO array for 5G mobile phones based on the theory of characteristic modes of composite PEC-lossy dielectric structures. *IEEE Trans Antenn Propag*, 70(3):1623-1631. https://doi.org/10.1109/tap.2021.3133432

Zhang XX, Ren AD, Liu Y, 2020. Decoupling methods of MIMO antenna arrays for 5G applications: a review. *Front Inform Technol Electron Eng*, 21(1):62-71. https://doi.org/10.1631/FITEE.1900466

Zhao X, Yeo SP, Ong LC, 2018. Decoupling of inverted-F antennas with high-order modes of ground plane for 5G mobile MIMO platform. *IEEE Trans Antenn Propag*, 66(9):4485-4495. https://doi.org/10.1109/tap.2018.2851381